nature materials

LETTERS

https://doi.org/10.1038/s41563-020-0703-y

Check for updates

A biohybrid synapse with neurotransmitter-mediated plasticity

Scott T. Keene[1,7], Claudia Lubrano[2,3,7], Setareh Kazemzadeh[4], Armantas Melianas[1], Yaakov Tuchman[1], Giuseppina Polino[2,6], Paola Scognamiglio[2], Lucio Cinà[5], Alberto Salleo[1]✉, Yoeri van de Burgt[4]✉ and Francesca Santoro[2]✉

Brain-inspired computing paradigms have led to substantial advances in the automation of visual and linguistic tasks by emulating the distributed information processing of biological systems[1]. The similarity between artificial neural networks (ANNs) and biological systems has inspired ANN implementation in biomedical interfaces including prosthetics[2] and brain-machine interfaces[3]. While promising, these implementations rely on software to run ANN algorithms. Ultimately, it is desirable to build hardware ANNs[4,5] that can both directly interface with living tissue and adapt based on biofeedback[6,7]. The first essential step towards biologically integrated neuromorphic systems is to achieve synaptic conditioning based on biochemical signalling activity. Here, we directly couple an organic neuromorphic device with dopaminergic cells to constitute a biohybrid synapse with neurotransmitter-mediated synaptic plasticity. By mimicking the dopamine recycling machinery of the synaptic cleft, we demonstrate both long-term conditioning and recovery of the synaptic weight, paving the way towards combining artificial neuromorphic systems with biological neural networks.

Neuromorphic devices offer many of the same functionalities as biological synapses and are ideally suited for hardware ANNs, making them a promising bridge between artificial and biological neural networks[8,9]. Organic neuromorphic devices are particularly relevant for cell–device interfaces due to their biocompatibility, relatively low mechanical modulus and responsivity to analytes in the surrounding (aqueous) media[10–12]. Synaptic functions including short-term potentiation (STP) and global regulation of synaptic behaviour have been demonstrated in organic neuromorphic devices using polye thylenedioxythiophene:poly(styrene sulfonate) (PEDOT:PSS) as the active material[13]. In fact, PEDOT:PSS is also a viable surface for in vitro monitoring[14,15] and can also be exploited for the electrochemical detection of neurotransmitters through redox reactions[16].

Current neural interfaces utilize electronic devices that record local electric fields generated by both action potentials and synaptic currents and use electrical potentials to modulate depolarization processes at both the single-cell level and network hubs[17–19]. In previous work, neuromorphic devices have been connected to the electrical outputs of cells to regulate the 'synaptic weight' of the device[20,21]. Furthermore, microelectrode array recordings of neuronal cultures have been sorted and processed using inorganic memristors[22] or field-programmable-gate-array-based neural networks[23]. Long-term connectivity between neurons in biological systems, however, is governed by chemical signals from neurotransmitter release into the synapse. Thus, to emulate biological synaptic behaviour, the connectivity (such as synaptic weight) of the neuromorphic device must be dynamically regulated by the local neurotransmitter activity.

In this work, we report a functional biohybrid synapse comprising a dopaminergic presynaptic domain of PC-12 cells coupled to an organic neuromorphic device as the postsynaptic domain (Fig. 1a–d). Dopamine plays an important role in regulating synaptic transmission from cell to cell[24]. In particular, dopamine regulates synaptic plasticity, affecting synaptic conditioning such as long-term potentiation (LTP) and depression (LTD)[25]. The importance of dopamine signalling in the modulation of synaptic connectivity makes it an ideal model to demonstrate the regulation of synaptic weights in neuromorphic-based prosthetics.

In our biohybrid synapse, dopamine exocytosed by PC-12 cells at the presynaptic end is locally oxidized at the postsynaptic gate electrode (Fig. 1b). Following dopamine oxidation, the resulting change in the charge state of the gate electrode induces ion flow in the aqueous electrolyte, thus altering the conductance of the postsynaptic channel, as explained in the literature (ref. [11]). The dopamine oxidation process emulates the postsynaptic receptor binding observed in biological synapses, while the modified channel conductance emulates synaptic weight modulation by the neurotransmitter. When dopamine is present in solution, the change in the synaptic weight of the postsynaptic channel consists of both a short- and a long-term component (Fig. 1e). Indeed, the flow of ions under the applied postsynaptic gate bias results in short-term modulation of the postsynaptic channel conductance (independent of dopamine concentration) as previously reported[26], whereas dopamine oxidation results in long-term conditioning of the neuromorphic channel. In biological synapses, dopamine binding to postsynaptic receptors is reversible. Dopamine can return to the presynaptic end through endocytic recycling pathways[27]. Here, this process is emulated by a polydimethylsiloxane (PDMS) microfluidic channel, which facilitates the recycling of dopamine and its oxidation product, dopamine *o*-quinone[28], at the artificial synapse (Fig. 1c,d).

When using the cell culture media as an electrolyte (in the absence of cells and absence of dopamine), a voltage pulse at the gate electrode (V_{post}) results in the reversible (short-term) change in conductance of the PEDOT:PSS neuromorphic channel due to

[1]Department of Materials Science and Engineering, Stanford University, Stanford, CA, USA. [2]Tissue Electronics, Istituto Italiano di Tecnologia, Naples, Italy. [3]Dipartimento di Chimica, Materiali e Produzione Industriale, Università di Napoli Federico II, Naples, Italy. [4]Microsystems, Institute for Complex Molecular Systems, Eindhoven University of Technology, Eindhoven, The Netherlands. [5]Cicci Research, Grosseto, Italy. [6]Present address: Dipartimento di Ingegneria Elettronica, Università 'Tor Vergata', Roma, Italy. [7]These authors contributed equally: Scott T. Keene, Claudia Lubrano. ✉e-mail: asalleo@stanford.edu; y.b.v.d.burgt@tue.nl; francesca.santoro@iit.it

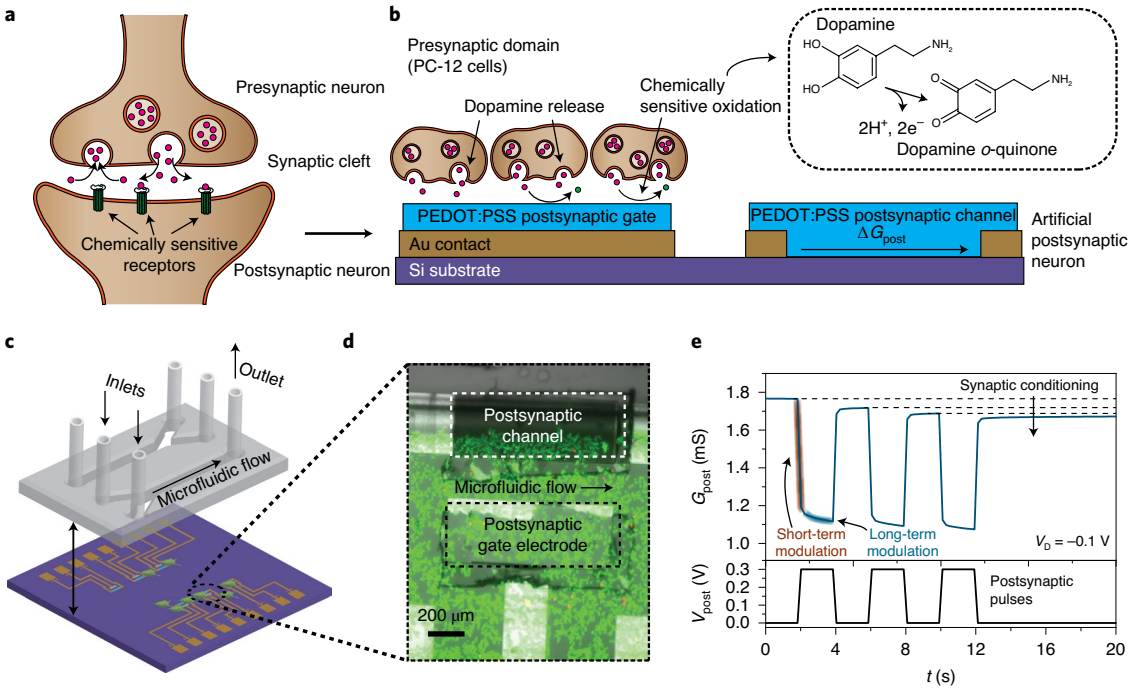

Fig. 1 | Design and performance of dopamine-mediated organic neuromorphic device. a,**b**, Schematic comparison of a biological synapse (**a**) and our neurotransmitter-mediated neuromorphic device (**b**). The oxidation of dopamine (pink spheres) to dopamine *o*-quinone (green spheres) at the postsynaptic gate electrode controls the change in conductance of the postsynaptic channel. **c**, Schematic showing the neuromorphic device array with microfluidic channels used for dopamine flow. **d**, Inset showing a fluorescence image of PC-12 cells coupled to a single device. **e**, Short-term and long-term modulation of the postsynaptic conductance (G_{post}) under dopamine flow (in the absence of cells) achieved using voltage pulses at the postsynaptic gate (V_{post} = +0.3 V, t_{post} = 2 s). G_{post} was measured using a source–drain voltage V_D = −0.1 V.

ion flow into the channel changing its doping state (Supplementary Fig. 1)[10,29]. When dopamine is introduced into the electrolyte solution, the conductance change is enhanced due to the oxidation of dopamine at the postsynaptic gate electrode (Extended Data Fig. 1)[16]. Crucially, unlike when only the cell culture media is present, the conductance change resulting from dopamine oxidation is permanent as a result of the irreversibility of this reaction (Extended Data Fig. 2). Thus, electrons flowing from dopamine to the postsynaptic gate electrode under an applied potential V_{post} cannot flow back to solution even when V_{post} is returned to 0 V (Extended Data Figs. 3 and 4). The resulting permanent change in channel conductance (Fig. 1e) emulates long-term potentiation in biological neural networks. In fact, in nature, long-term modulation only happens when neurotransmitter molecules are present in the synaptic cleft following vesicle exocytosis (that is, after postsynaptic pulses are fired) by the presynaptic cell. Thus, our biohybrid synapse emulates the Hebbian learning rule[7]: 'neurons that fire together, wire together'.

Fluorescence imaging revealed that PC-12 cells survived on neuromorphic devices with no relevant toxicity effects (Fig. 1e and Extended Data Fig. 5) and actively secreted dopamine following plating[30]. The dopamine secreted by a 20% confluent monolayer is detected at the postsynaptic domain by sweeping the postsynaptic gate voltage, V_{post}, and monitoring the conductance of the postsynaptic channel, $G_{post} = I_{ch}/V_{ch}$, where I_{ch} and V_{ch} are the current and voltage applied across the postsynaptic channel, respectively (Fig. 2a, solid lines). Since the PC-12 cell monolayer collectively constitutes the presynaptic domain, different cell densities influence the overall dopamine accumulation. As expected, a higher cell density (30% confluent monolayer) leads to an increased peak transconductance, g_m (Fig. 2a, dashed lines), indicating an increase in dopamine concentration oxidizing at the postsynaptic gate electrode surface (Extended Data Fig. 1). Further increase of the cell density to a 90% confluent monolayer creates a diffusion barrier, preventing the efficient circulation and oxidation of dopamine at the gate electrode (Supplementary Fig. 2). Thus, we utilized a 70% cell monolayer for device demonstrations. We found that the long-term viability of cells extends to at least 24 h (Extended Data Fig. 6), confirming the stability of the biohybrid synapse.

To efficiently emulate the synaptic cleft, the neuromorphic device must be able to respond to the dynamic release and recycling of small absolute counts of neurotransmitter. In a biological synapse, this is achieved by the formation of a junction, which slows dopamine diffusion away from the synaptic cleft, resulting in accumulation of the neurotransmitter. Similarly, our biohybrid synapse also relies on the junction between the pre- and postsynaptic domains. We visualized the junction between PC-12 cells and the surface of the postsynaptic gate electrode using cross-sectional scanning electron microscopy with focused ion-beam milling (FIB/SEM; Fig. 2b; see Methods) to characterize their physical coupling[31]. The interspace between the plasma membrane of dopaminergic cells (presynaptic domain) and the PEDOT:PSS electrode (postsynaptic domain) constitutes the biohybrid synaptic cleft with an average spacing of 100 nm and minimum distance points of 5–10 nm, which is comparable to previous reports[32] (Fig. 2c). To emulate the synaptic recycling process of endocytosis, we flowed fresh solution through the microfluidic channel (Fig. 1c), which accelerated the diffusion of dopamine away from the synaptic cleft.

To demonstrate the dynamic behaviour of the biohybrid synapse under microfluidic flow, we measured the postsynaptic conductance (G_{post}) under a constant postsynaptic gate potential (V_{post} = 0.3 V) at different flow rates (Fig. 2d). At low flow rates (light blue), the postsynaptic conductance decreases steadily due

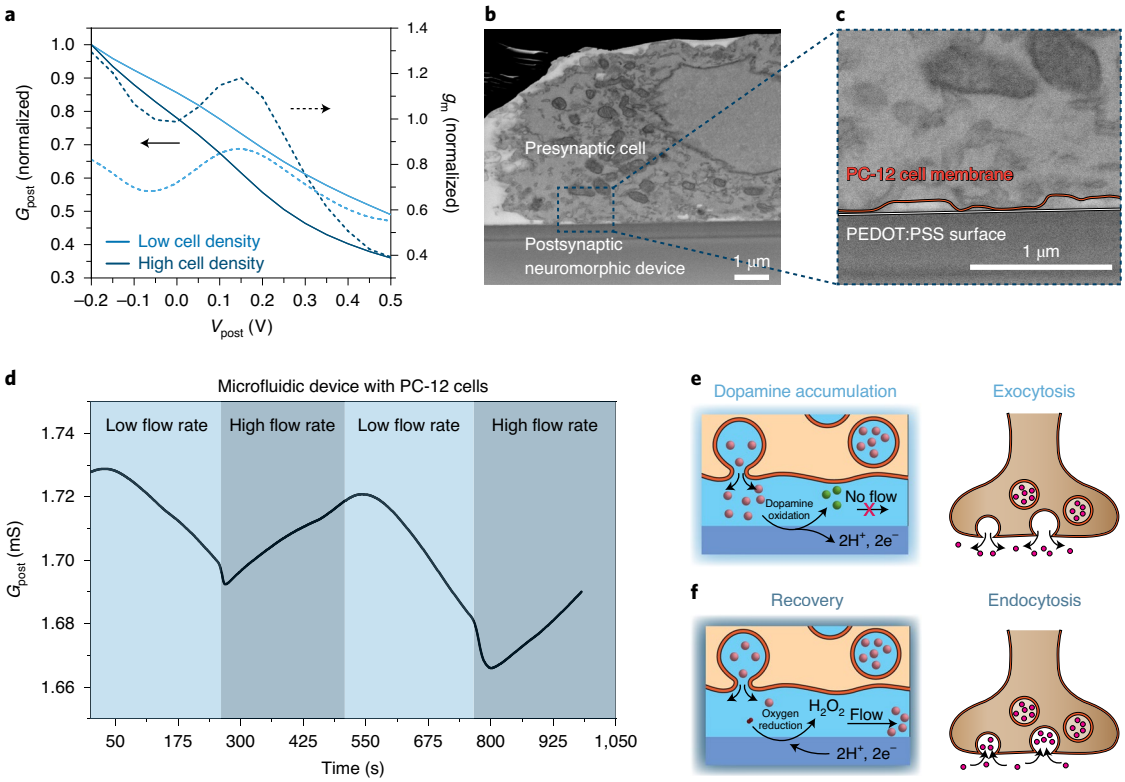

Fig. 2 | Measurement of dopamine released by PC-12 cells. a, Normalized transfer characteristics and transconductance of the neuromorphic device with PC-12 cells at low and high cell densities (light and dark blue, respectively). **b**, Cross-sectional SEM image of a PC-12 cell plated on PEDOT:PSS obtained using FIB. **c**, Inset highlighting the cell membrane (orange) to electrode (white) interface. **d**, Dynamic behaviour of the neuromorphic device under a constant postsynaptic gate voltage V_{post} = +0.3 V and under microfluidic flow. **e**,**f**, Schematic representations of device behaviour (left) and emulated biological process (right) corresponding to the low flow rate (**e**) and high flow rate (**f**) shown in **d**. Accumulation of dopamine at the cell–PEDOT:PSS interface occurs under a low flow rate (**e**), which leads to memory conditioning due to the continuous oxidation of dopamine at the postsynaptic gate electrode surface. Under the high flow rate (**f**), removal of dopamine from the cell–PEDOT:PSS interface followed by reduction of oxygen leads to memory recovery, emulating endocytosis. ox., oxidation; red., reduction.

to the continuous build-up and oxidation of exocytosed dopamine (Fig. 2e). At high flow rates (dark blue), on the other hand, when dopamine is washed away from the surface before it can accumulate, G_{post} increases steadily because dopamine is cleared from the cleft and microfluidic channel before it can oxidize, emulating endocytosis (Fig. 2f). Previous reports have shown that dissolved oxygen can oxidize reduced PEDOT:PSS (ref. [33]), which results in the observed conductance increase (see Supplementary Text 1). Thus, the behaviour observed in Fig. 2d is attributed to the competing effects of dopamine oxidation and dissolved oxygen reduction (Extended Data Fig. 7). The result is a form of dynamic synaptic plasticity where the postsynaptic channel conductance (or synaptic weight) depends on the relative rates of dopamine release (in the biohybrid synaptic cleft) and oxidation versus dopamine recycling and oxygen reduction.

Finally, we demonstrated dopamine-mediated long-term conditioning at the postsynaptic end of the synapse. Dopamine released by presynaptic cells was oxidized by postsynaptic gate pulses (V_{post} = 0.3 V, t_{post} = 2 s, n = 15 pulses), resulting in a permanent decrease of the postsynaptic conductance G_{post} (Fig. 3a) of 8.4 ± 2.8 μS per pulse. From the calibration curves (Extended Data Fig. 8), we estimate a dopamine concentration (C_{DA}) of ~10–15 μM within the biohybrid synaptic cleft. We confirm the successful long-term conditioning of the postsynaptic domain, G_{post}, (that is, the modulation of the synaptic weight) by measuring G_{post} after PC-12 cell incubation for an additional two hours. The conductance level does not increase following the second incubation, showing that the conditioning of the synaptic weight G_{post} is retained, thus confirming successful long-term conditioning of the postsynaptic domain. There is a slight decrease in conductivity due to the drift in the baseline conductance during cell incubation (Supplementary Fig. 3), but the relevant synaptic behaviour is retained. To verify the continued synaptic plasticity, we repeated the pulsing measurements with the same conditions after four hours of incubation (Fig. 3a, dark blue). During this time, dopamine continued to accumulate in the extracellular media, resulting in a 40% larger long-term conditioning ΔG_{post} (11.8 ± 4 μS, C_{DA} of ~15–20 μM) in response to postsynaptic pulses, further showing the dynamic response of the biohybrid synapse to presynaptic dopamine signalling.

Similar to the biological connectivity of neurons, the reported neuromorphic device response is related to the rates of dopamine release at the postsynaptic interface as well as the diffusion (or endocytosis) rates of the neurotransmitter away from the interface. Under pulsed operation, the biohybrid synapse follows the Hebbian model for synaptic connectivity: dopamine is present at the synaptic interface for a short period of time following an action potential, but the pulsing of the postsynaptic domain is required to achieve long-term conditioning. This effect is demonstrated by stimulating PC-12 cells with KCl solution to elicit exocytosis and monitoring the device response to postsynaptic pulses (Fig. 3b,c). Without sufficient stimulation (60 mM KCl), the dopamine release rate of PC-12 is too slow to accumulate during the short timescale (~2 min) of the measurement, and thus no device response is observed during pulsing (Fig. 3b). By contrast, when the stimulation of PC-12 cells

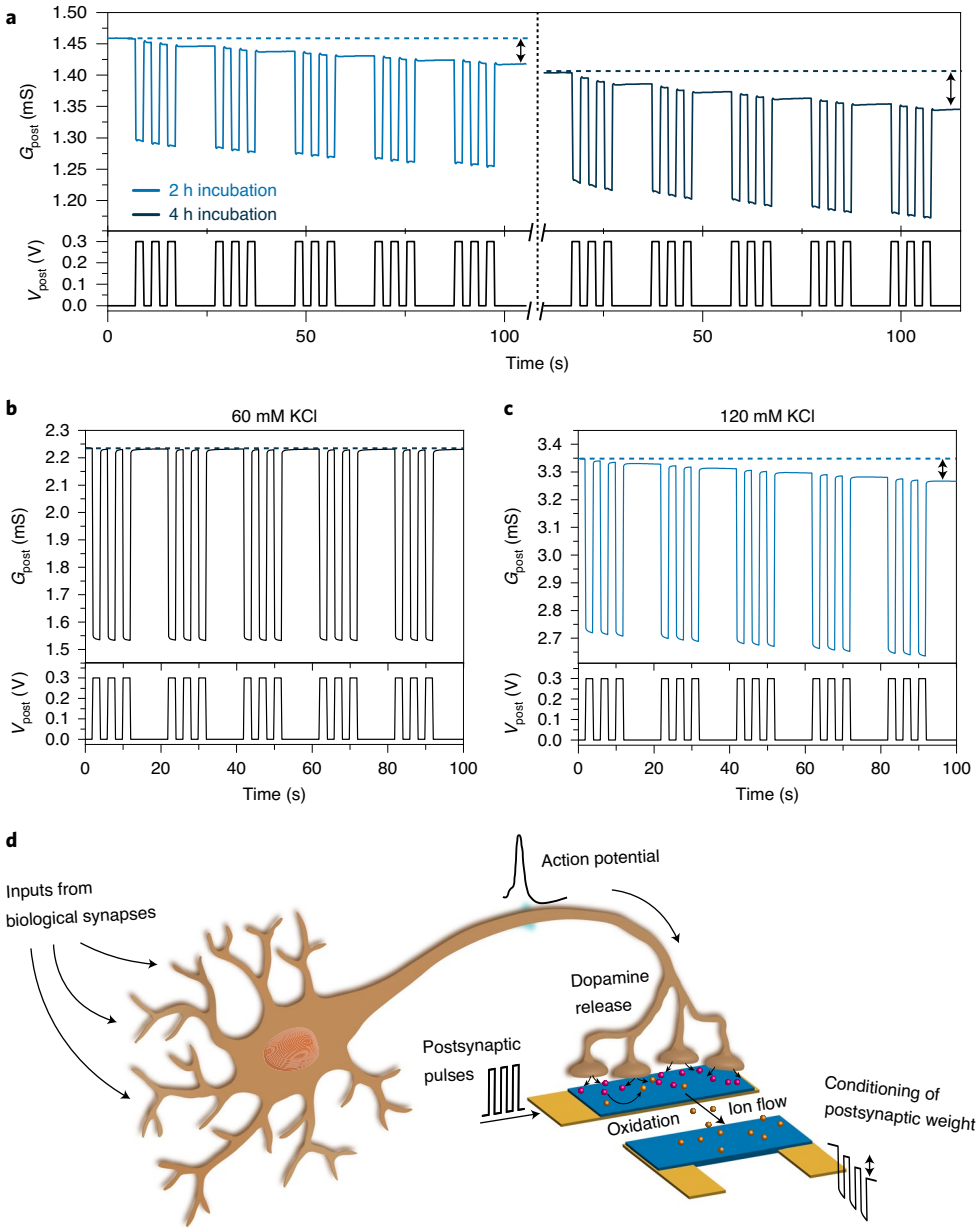

Fig. 3 | Long-term potentiation of the artificial postsynaptic neuron. a, Synaptic conditioning of the neuromorphic device coupled with PC-12 dopaminergic cells resulting from the oxidation of accumulated dopamine at the cell–PEDOT:PSS interface during 2 h (light blue) and 4 h (dark blue) of incubation. **b**,**c**, Biohybrid synapses coupled with PC-12 cells were measured following removal of the extracellular solution and washout of the channel followed by addition of a 60 mM KCl solution (**b**) and a 120 mM KCl solution (**c**) to elicit exocytosis in the PC-12-cell layer. The change in conductivity in response to postsynaptic voltage pulses occurs only when PC-12 cells are stimulated with 120 mM KCl due to the high release rate of dopamine, whereas the dopamine release after 60 mM KCl stimulation is insufficient to elicit a device response. **d**, Schematic drawing of the potential integration of an artificial neuron with a biological neuron. In the case of a neuron, the dopamine concentration at the device–cell interface depends on the firing rate of the presynaptic neuron, while the change in postsynaptic current (or long-term potentiation) depends on the pulse rates of both the presynaptic and postsynaptic domains, resulting in a correlated spiking learning mechanism.

is increased (120 mM KCl), the postsynaptic voltage pulses elicit long-term conditioning of the device of ΔG_{post} of 5.4 ± 0.8 µS per pulse (Fig. 3c), comparable to the results in Fig. 3a. Thus, the synaptic weight of the neuromorphic device is modulated by the postsynaptic pulses in tandem with the rapid dopamine release from the presynaptic domain, thereby regulating the long-term synaptic weight of the neuromorphic channel in an analogous fashion to biological neurons (Fig. 3d). The neurotransmitter-mediated neuromorphic device presented in this work constitutes a fundamental building block for ANNs that can be directly modulated based on biological feedback from live neurons and is a crucial first step in realizing next-generation adaptive biohybrid interfaces.

In the future, we expect that through further downscaling of the neuromorphic devices used in this work, detection limits could be reduced to the scale of single-vesicle release events (see Extended Data Fig. 9 and Supplementary Text 2). One of the remaining challenges is designing the connectivity between the biohybrid neuromorphic devices and processing units. We expect that biohybrid devices presented here can be used to bridge synaptic connections and could further be utilized in conjunction with organic ANN

circuits separate from the biohybrid interface for additional signal processing. Additionally, we envision that by combining biohybrid synapses with stimulating devices such as electrochemical ion pumps[34] to form a prosthetic synaptic junction, systems in the far future could introduce or repair chemical communication between neurons.

Online content

Any methods, additional references, Nature Research reporting summaries, source data, extended data, supplementary information, acknowledgements, peer review information; details of author contributions and competing interests; and statements of data and code availability are available at https://doi.org/10.1038/s41563-020-0703-y.

Received: 29 October 2019; Accepted: 11 May 2020;
Published online: 15 June 2020

References

1. Furber, S. Large-scale neuromorphic computing systems. *J. Neural Eng.* **13**, 051001 (2016).
2. Grahn, P. J. et al. Restoration of motor function following spinal cord injury via optimal control of intraspinal microstimulation: toward a next generation closed-loop neural prosthesis. *Front. Neurosci.* **8**, 1–12 (2014).
3. Bonifazi, P. et al. In vitro large-scale experimental and theoretical studies for the realization of bi-directional brain-prosthese. *Front. Neural Circuits* **7**, 1–19 (2013).
4. van Doremaele, E. R. W., Gkoupidenis, P. & van de Burgt, Y. Towards organic neuromorphic devices for adaptive sensing and novel computing paradigms in bioelectronics. *J. Mater. Chem. C* https://doi.org/10.1039/C9TC03247A (2019).
5. Fuller, E. J. et al. Parallel programming of an ionic floating-gate memory array for scalable neuromorphic computing. *Science* **364**, 570–574 (2019).
6. Berco, D. & Shenp Ang, D. Recent progress in synaptic devices paving the way toward an artificial cogni-retina for bionic and machine vision. *Adv. Intell. Syst.* **1**, 1900012 (2019).
7. Hebb, D. O. *The Organization of Behavior: a Neuropsychological Theory* (Wiley, 1949).
8. Vassanelli, S. & Mahmud, M. Trends and challenges in neuroengineering: toward 'intelligent' neuroprostheses through brain-'brain inspired systems' communication. *Front. Neurosci.* **10**, 438 (2016).
9. Chiolerio, A., Chiappalone, M., Ariano, P. & Bocchini, S. Coupling resistive switching devices with neurons: state of the art and perspectives. *Front. Neurosci.* **11**, 70 (2017).
10. Rivnay, J. et al. Organic electrochemical transistors. *Nat. Rev. Mater.* **3**, 17086 (2018).
11. van de Burgt, Y. et al. A non-volatile organic electrochemical device as a low-voltage artificial synapse for neuromorphic computing. *Nat. Mater.* **16**, 414–418 (2017).
12. van de Burgt, Y., Melianas, A., Keene, S. T., Malliaras, G. & Salleo, A. Organic electronics for neuromorphic computing. *Nat. Electron.* **1**, 386–397 (2018).
13. Gkoupidenis, P., Koutsouras, D. A. & Malliaras, G. G. Neuromorphic device architectures with global connectivity through electrolyte gating. *Nat. Commun.* **8**, 15448 (2017).
14. Asplund, M. et al. Toxicity evaluation of PEDOT/biomolecular composites intended for neural communication electrodes. *Biomed. Mater.* **4**, 045009 (2009).
15. Santoro, F., van de Burgt, Y., Keene, S. T., Cui, B. & Salleo, A. Enhanced cell-chip coupling by rapid femtosecond laser patterning of soft PEDOT:PSS biointerfaces. *ACS Appl. Mater. Interfaces* **9**, 39116–39121 (2017).
16. Gualandi, I. et al. Selective detection of dopamine with an all PEDOT:PSS organic electrochemical transistor. *Sci. Rep.* **6**, 2–5 (2016).
17. Obaid, A. M. et al. Massively parallel microwire arrays integrated with CMOS chips for neural recording. *Sci. Adv.* **6**, 573295 (2020).
18. Khodagholy, D. et al. NeuroGrid: recording action potentials from the surface of the brain. *Nat. Neurosci.* **18**, 310–315 (2015).
19. Hess, L. H. et al. Electrical coupling between cells and graphene transistors. *Small* **11**, 1703–1710 (2015).
20. Juzekaeva, E. et al. Coupling cortical neurons through electronic memristive synapse. *Adv. Mater. Technol.* **4**, 4–9 (2019).
21. Serb, A. et al. Memristive synapses connect brain and silicon spiking neurons. *Sci. Rep.* **10**, 2590 (2020).
22. Gupta, I. et al. Sub 100 nW volatile nano-metal-oxide memristor as synaptic-like encoder of neuronal spikes. *IEEE Trans. Biomed. Circuits Syst.* **12**, 351–359 (2018).
23. Buccelli, S. et al. A neuromorphic prosthesis to restore communication in neuronal networks. *iScience* **19**, 402–414 (2019).
24. Burns, M. E. & Augustine, G. J. Synaptic structure and function: dynamic organization yields architectural precision. *Cell* **83**, 187–194 (1995).
25. Calabresi, P., Picconi, B., Tozzi, A. & di Filippo, M. Dopamine-mediated regulation of corticostriatal synaptic plasticity. *Trends Neurosci.* **30**, 211–219 (2007).
26. Gkoupidenis, P., Schaefer, N., Strakosas, X., Fairfield, J. A. & Malliaras, G. G. Synaptic plasticity functions in an organic electrochemical transistor. *Cit. Appl. Phys. Lett.* **107**, 263302 (2015).
27. Li, Y. et al. Identification of two functionally distinct endosomal recycling pathways for dopamine D_2 receptor. *J. Neurosci.* **32**, 7178–7190 (2012).
28. Shahrokhian, S. & Bozorgzadeh, S. Electrochemical oxidation of dopamine in the presence of sulfhydryl compounds: application to the square-wave voltammetric detection of penicillamine and cysteine. *Electrochim. Acta* **51**, 4271–4276 (2006).
29. Keene, S. T. et al. Optimized pulsed write schemes improve linearity and write speed for low-power organic neuromorphic devices. *J. Phys. D Appl. Phys.* **51**, 224002 (2018).
30. Yakushenko, A., Kätelhön, E. & Wolfrum, B. Parallel on-chip analysis of single vesicle neurotransmitter release. *Anal. Chem.* **85**, 5483–5490 (2013).
31. Li, X. et al. A nanostructure platform for live-cell manipulation of membrane curvature. *Nat. Protoc.* **14**, 1772–1802 (2019).
32. Santoro, F. et al. Revealing the cell-material interface with nanometer resolution by focused ion beam/scanning electron microscopy. *ACS Nano* **11**, 8320–8328 (2017).
33. Keene, S. T., Melianas, A., van de Burgt, Y. & Salleo, A. Mechanisms for enhanced state retention and stability in redox-gated organic neuromorphic devices. *Adv. Electron. Mater.* **5**, 1800686 (2018).
34. Isaksson, J. et al. Electronic control of Ca^{2+} signalling in neuronal cells using an organic electronic ion pump. *Nat. Mater.* **6**, 673–679 (2007).

Methods

Neuromorphic device fabrication. Neuromorphic device photolithographic patterning was performed on silicon wafers with a 200 nm thermal oxide. First, metal interconnects (5/100 nm Ti/Au) were patterned using a standard lift-off process. The wafers were subsequently coated with 1.5 µm of Parylene-C as the insulating layer, which was crosslinked using a treatment of 3-(trimethoxysilyl) propyl methacrylate to promote adhesion to the substrate. Following the first Parylene-C layer, a dilute soap (3% Micro-90 in deionized water) solution was spin-cast on top, followed by deposition of a second Parylene-C layer, later used as a peel-off layer. The wafers were then coated with 75 nm of Ti using e-beam evaporation, photolithographically patterned and dry etched to define the neuromorphic channel and postsynaptic gate areas. The wafer dies were cleaned with isopropanol sonication followed by ultraviolet–ozone cleaning before spin-coating the polymer layer. PEDOT:PSS (Hereaus, Clevios PH 1000) aqueous solution was prepared by adding 6 vol.% ethylene glycol (Sigma-Aldrich) to increase the PEDOT:PSS conductivity, 0.1 vol.% dodecylbenzene sulfonic acid (Sigma-Aldrich) as a surfactant, and 1 vol.% (3-glycidyloxypropyl)trimethoxysilane (Sigma-Aldrich) as a crosslinking agent to improve mechanical stability. PEDOT:PSS solution was spun on the wafer die at 1,000 r.p.m. for 2 min and baked at 120 °C for 20 min. The top Parylene-C layer was then peeled off to retain PEDOT:PSS only in the photolithographically defined neuromorphic channel and postsynaptic gate areas. The wafer dies were gently rinsed in deionized water to eliminate residual soap and were subsequently dried at 120 °C for 5 min.

Microfluidic device fabrication and integration. Microfluidic channels were prepared using a photolithographically patterned mould in SU-8 epoxy resin (~1 mm thick) on an undoped silicon wafer. PDMS was mixed with a crosslinker in a ratio of 10:1 wt/wt and degassed in a vacuum desiccator before being poured onto the wafer containing the mould and heated to 80 °C for 24 h to cure. A 1.2-mm-diameter biopsy punch was used to create the holes for inlets and outlets, which consisted of Teflon tubing (0.813 mm inner diameter, 1.32 mm outer diameter). A small amount of uncured PDMS was used to coat the bottom surface of the PDMS microfluidic channel before placing it onto the silicon substrate, which was subsequently baked at 80 °C for 1 h.

Dopamine solution preparation. Dopamine solutions were prepared by dissolving dopamine hydrochloride (98%, Sigma-Aldrich) into either 100 mM sodium chloride (NaCl) aqueous solution or into cell culture media (Dulbecco's Modified Eagle's Medium (DMEM)—high glucose, Sigma-Aldrich) at a concentration of 200 µM. To vary the concentration in the microfluidic experiments, the 200 µM dopamine solution was mixed with a 0 µM dopamine solution to dilute to the desired concentration using the two inlets of the microfluidic channel. All dopamine solutions were prepared immediately before measurements to avoid degradation due to ultraviolet exposure.

Characterization of artificial postsynaptic devices. Devices were characterized using a commercial platform (ARKEO, Cicci Research) composed of a thermal controlled stage, two-channel source meter units and two synchronized microfluidic pumps. Spring contact probes were used to access the postsynaptic gate and drain electrodes. Microfluidic fluid flow across the device was controlled using two microfluidic pumps (Syringepump) controlled by custom LabView software. Transfer curves were taken by sweeping the postsynaptic electrode voltage from −0.2 V to +0.8 V. To calibrate with increasing dopamine, the concentration in solution was controlled by the two inlets of the microfluidic channel (one without dopamine, the other containing 0.2 mM of dopamine) to mix dopamine to the desired concentration using a constant flow rate of 0.2 ml min^{-1}. Pulsed measurements were performed using a set of voltage pulses (V_{post} = +0.3 V) applied to the postsynaptic electrode while monitoring the postsynaptic current (V_{read} = −0.1 V).

Cell culture, biocompatibility and dopamine immunohistochemistry. The experiments were performed using a catecholamine-containing rat pheochromocytoma cell line (PC-12). PC-12 cells were cultured in a 25 mm^2 flask in DMEM media (Sigma-Aldrich) supplemented with 10% fetal bovine serum (Sigma-Aldrich), 1% penicillin/streptomycin (Sigma-Aldrich) and 1% L-glutamine (Sigma-Aldrich), in a 5% CO_2 incubator at 37 °C. Confluent PC-12 cells were trypsinated and cells were seeded on planar PEDOT substrates at a density of 150,000 cells cm^{-2} and left in the incubator at 37 °C for 24 h. To assess the biocompatibility, cells were stained with a solution of calcein-AM (the acetomethoxy derivate of calcein; Sigma-Aldrich, final concentration 1 ug ml^{-1}) and propidium iodide (Thermo Fisher Scientific, final concentration 10 µg ml^{-1}) in PBS buffer and incubated at 37 °C for 10 min.

Cell morphology was analysed through actin staining with phalloidin-647 (Life Technologies), while the dopamine secretion was verified through immunohistochemistry, employing as the primary antibody a dopamine monoclonal antibody (Thermo Fisher Scientific) and Alexa Fluor-488 anti-mouse (Thermo Fisher Scientific) as the secondary antibody; nuclei were stained with Hoechst (Thermo Fisher Scientific). For the staining procedure, cells were fixed in paraformaldehyde 4% (SIC) for 15 min at room temperature and then washed several times with phosphate buffered saline (PBS, Sigma-Aldrich). The cell membrane was permeabilized through incubation with Triton-X (Sigma-Aldrich, 0.1%) in PBS for 5 min at room temperature, followed by a blocking step of 45 min with PBS containing 2% of bovine serum albumin (BSA, Sigma-Aldrich). Substrates were then incubated for 1 h at room temperature with the primary antibody, which was diluted 1:100 in PBS containing 1% BSA (PBB). The following steps were the incubation with the secondary antibody (diluted 1:500 in PBB) and then with phalloidin-647 (diluted 1:100 in PBB); both dyes were incubated for 30 min at room temperature. Finally, the nuclei staining was performed through incubation with Hoechst (diluted 1:5,000 in PBS) for 15 min. The substrates were imaged with an Axiobserver-Z1 (Zeiss) using a magnification of ×10 (for the biocompatibility experiment) and ×40 (for the cell morphology analysis).

Embedding procedure of ultra-thin resin for SEM and FIB/SEM. Cells were washed with 0.1 M sodium cacodylate buffer (Electron Microscopy Science) and fixed overnight with 3.5% glutaraldehyde at 4 °C. The fixative solution was removed and the substrates were washed three times with chilled distilled water. Then, cells were treated with a reduced osmium procedure (RO-T-O) as previously reported[31]. Afterwards, cells were dehydrated with an ethanol (Electron Microscopy Science) series from 30% to 100% (5 min each). Epoxy resin was slowly allowed to penetrate the cells starting with an ethanol/resin ratio of 3:1, then a ratio of 1:1 and finally 1:3 (3 h each). The last step consisted of cells penetrated only with resin for at least 3 h. The excess resin was drained out, and the final polymerization was achieved at 60 °C overnight[31]. Samples were mounted on a SEM stub with colloidal silver paste and a thin layer of gold–palladium was sputtered on top of each sample.

FIB sectioning. The samples were placed in a dual-beam machine (Helios 600i, Thermo Fisher Scientific). SEM images were acquired using a voltage in the range of 3–5 kV and currents from 21 pA to 1.4 nA. The sectioning process was done on a target area that was covered with a protection layer of platinum (0.5 µm by electron-beam-induced deposition and 1 µm by ion-beam-induced deposition). A first trench was created to remove a large part of the material with a high voltage–current (30 kV, 0.79 nA), while a fine polishing was carried out at 30 kV and 80 pA. Once the cross-section was created, the images were acquired with a backscattered detector[31].

Dopamine detection measurements with PC-12 cells. A PDMS microfluidic channel (1 mm thick) was fixed to the neuromorphic device (length L = 750 µm, widht W = 270 µm), and the channel was sterilized with repeated washes of ethanol and sterile Milli-Q water. To enhance cell adhesion, the channel was filled with an aqueous solution of 0.1% collagen IV from human placenta (Sigma-Aldrich) for 1 h at 37 °C, and then washed with sterile Milli-Q water. Confluent PC-12 cells were trypsinated, and cells were seeded into the microfluidic channels (1 mm thick) at low cell density (770,000 cells cm^{-2}) and high cell density (1,540,000 cells cm^{-2}; Extended Data Fig. 5), and left in the incubator at 37 °C. The pulsed oxidation measurements were performed every 2 h to monitor the dopamine secretion process. For dynamic microfluidic flow measurements, PC-12 cells were plated with a density of 770,000 cells cm^{-2} and incubated for 4 h prior to performing the measurement. Microfluidic flow of warm (37 °C) DMEM cell culture solution was controlled using custom LabView software and manually updated during the measurement.

For KCl stimulation the PDMS microfluidic channel (1 mm thick) was fixed on the neuromorphic device (L = 30 µm, W = 10 µm), and treated with the same sterilization and coating protocols described above. Confluent PC-12 cells were trypsinated, and cells were seeded into the microfluidic channels (1 mm thick) at low cell density (770,000 cells cm^{-2}) and incubated for 4 h prior to performing the stimulation. The cell medium in the microfluidic channel was removed, and the channel was washed before adding a stimulating solution with a composition of 60 mM KCl or 120 mM KCl, 50 mM NaCl, 2 mM $CaCl_2$, 0.7 mM $MgCl_2$, 1 mM NaH_2PO_4 and 10 mM HEPES buffer (pH, 7.4). The pulsed measurement was performed immediately following addition of the KCl solution.

Data availability

The data represented in Figs. 1, 2 and 3 as well as Extended Data Figs. 1 through 9 are provided with the paper as source data. Other datasets generated and/or analysed during the current study are available from the authors on reasonable request.

Acknowledgements

A.S. and S.T.K. acknowledge financial support from the National Science Foundation and the Semiconductor Research Corporation, E2CDA Award no. 1739795. Additionally, S.T.K. thanks the Stanford Graduate Fellowship fund for support. A.M. gratefully acknowledges support from the Knut and Alice Wallenberg Foundation (KAW 2016.0494) for postdoctoral research at Stanford University. This work was in part performed at the Stanford Nano Shared Facilities (SNSF) and the nano@Stanford (SNF) labs, which are supported by the National Science Foundation

as part of the National Nanotechnology Coordinated Infrastructure under award ECCS-1542152. Y.v.d.B. gratefully acknowledges funding from the European Union's Horizon 2020 Research and Innovation Programme, grant agreement no. 802615. F.S. thanks the staff of the Cleanroom Facility at the Center Lab of Istituto Italiano di Tecnologia for the use of the dual-beam machine, and the group of A. Offenhäusser at the Institute of Complex Systems (ICS–8) of Jülich Forschungszentrum for providing the PC-12 cell line.

Author contributions

S.T.K., A.S., Y.v.d.B. and F.S. conceptualized the research and designed the experiments. S.T.K., C.L, S.K. and G.P. performed the experiments. A.M., Y.T. and S.T.K. designed and fabricated the neuromorphic devices. S.T.K., S.K. and Y.v.d.B. designed and fabricated the microfluidic channels. L.C. and S.T.K. designed and implemented the custom LabView analysis tools. S.T.K., C.L., A.S., Y.v.d.B. and F.S. analysed the data and prepared the manuscript.

Competing interests

The authors declare no competing interests.

Additional information

Extended data is available for this paper at https://doi.org/10.1038/s41563-020-0703-y.

Supplementary information is available for this paper at https://doi.org/10.1038/s41563-020-0703-y.

Correspondence and requests for materials should be addressed to A.S., Y.v.B. or F.S.

Reprints and permissions information is available at www.nature.com/reprints.

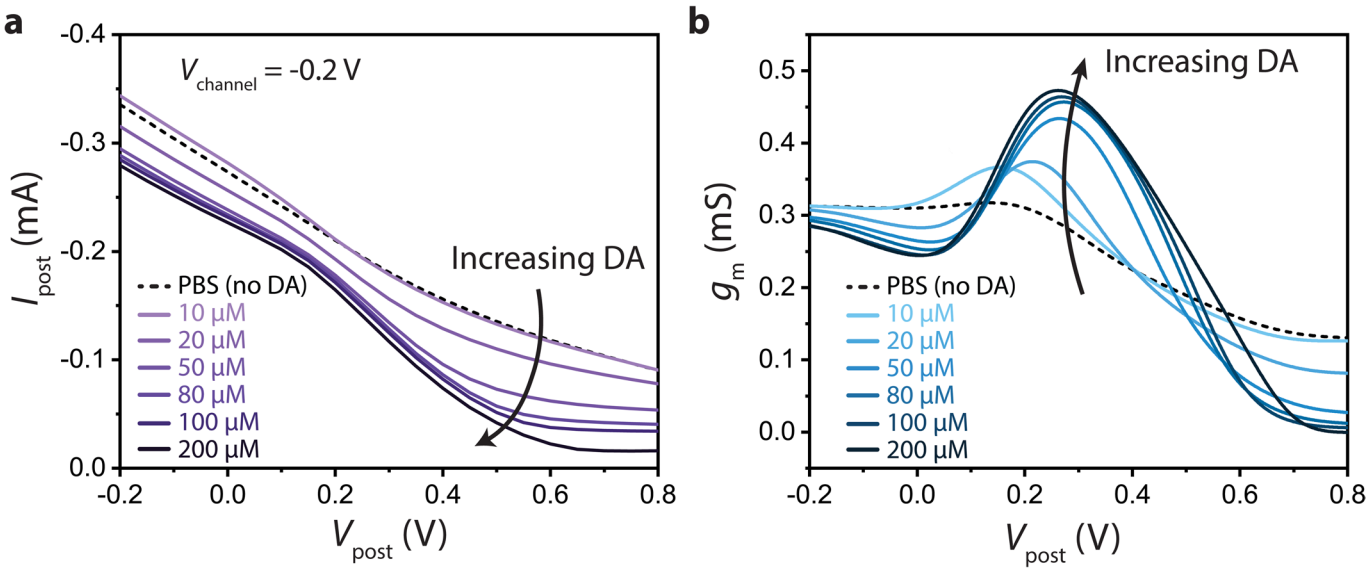

Extended Data Fig. 1 | Effect of dopamine concentration in cell culture media on neuromorphic device transfer characteristics. a, Transfer curves and **b**, corresponding transconductance curves as a function of dopamine concentration in DMEM solution flowed through the microfluidic channel showing an increase in peak transconductance at roughly +0.2 V corresponding to oxidation of dopamine.

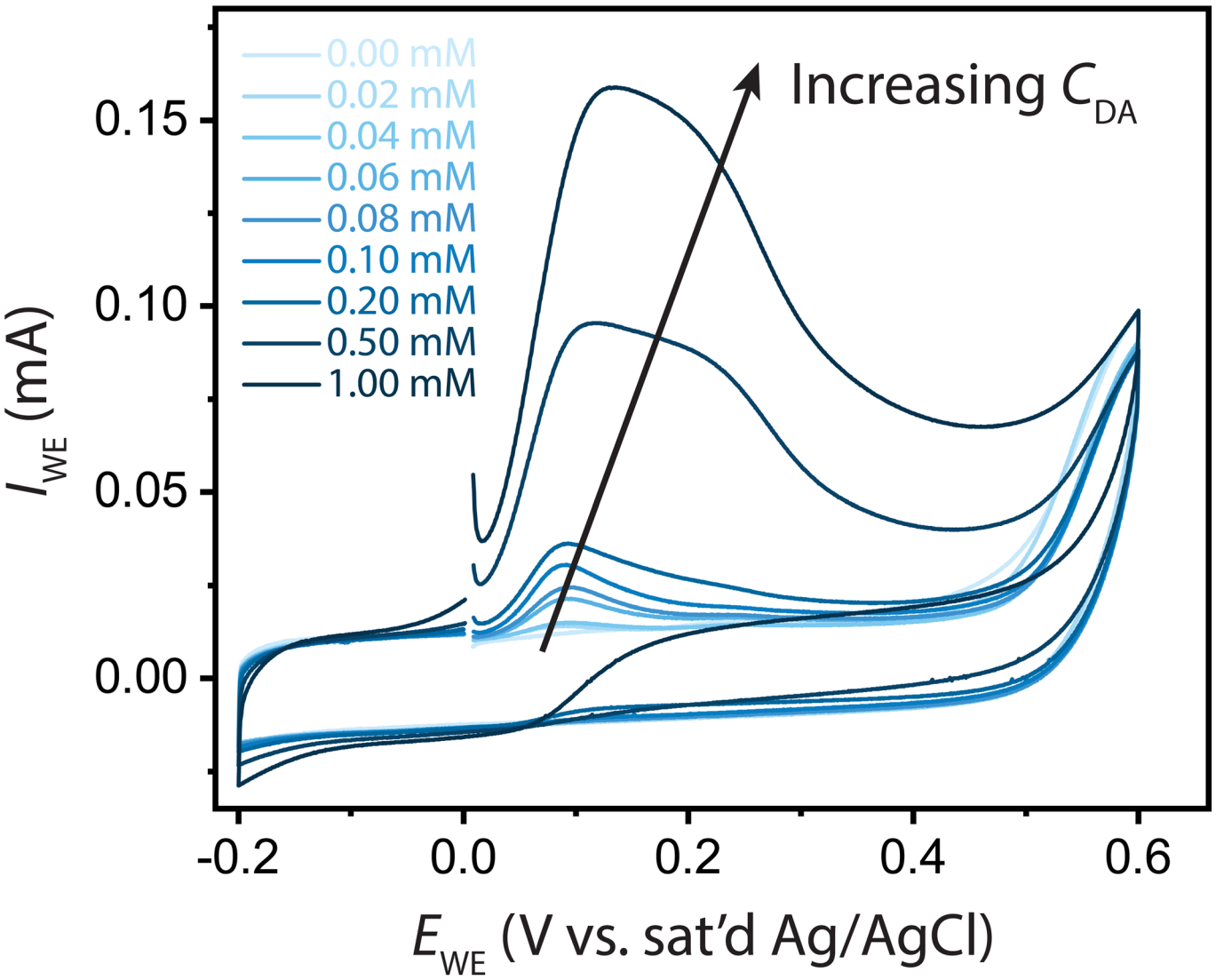

Extended Data Fig. 2 | Cyclic voltammetry (CV) of dopamine on PEDOT:PSS. CVs (scan rate = 10 mV·s^{-1}) show the oxidation of dopamine with a peak of ca. +0.1 V *vs* a saturated silver/silver chloride (sat'd Ag/AgCl) electrode for low dopamine concentrations (20–200 mM). At higher concentrations (0.5–1 mM), dopamine oxidation peak shifts and a secondary oxidation reaction is observed. The lack of a reduction peak in the reverse scan shows that the oxidation reaction is irreversible.

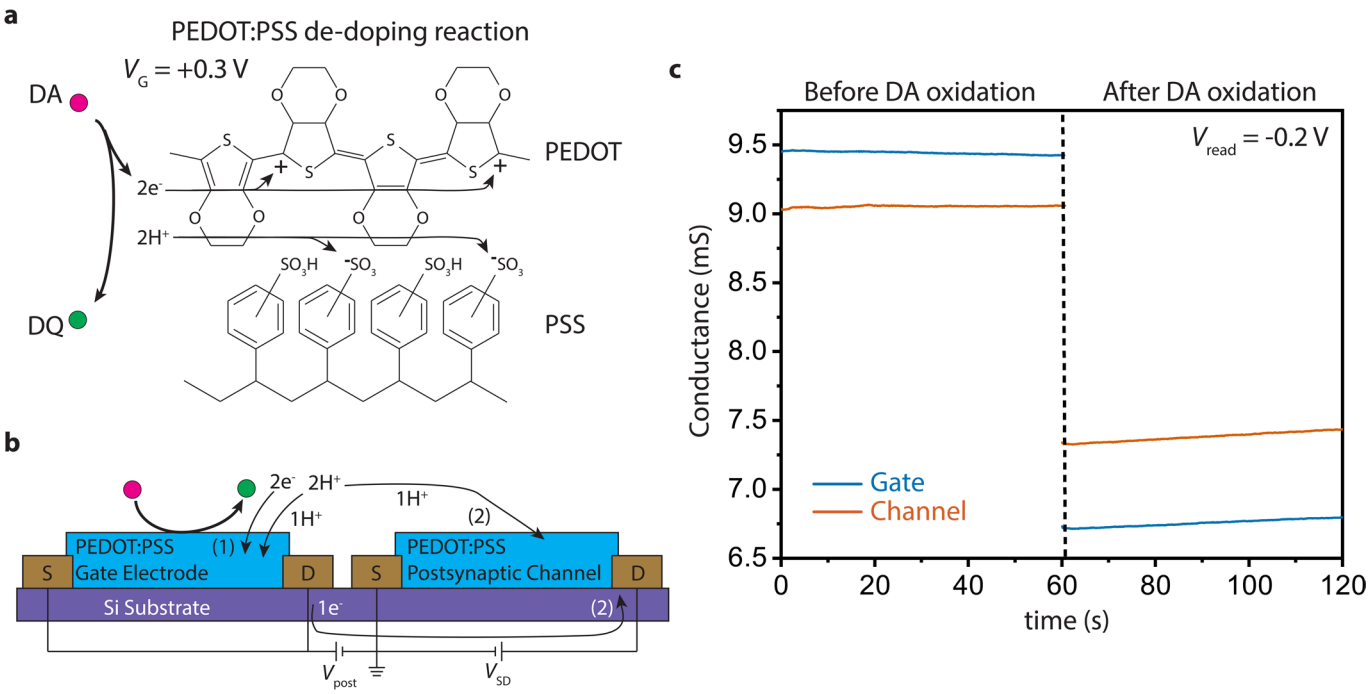

Extended Data Fig. 3 | Conductance modulation as a result of dopamine oxidation. a, When dopamine (DA, pink circles) is oxidized to dopamine *o*-quinone (DQ, green circles), the oxidation products ($2e^-$, $2H^+$) can compensate the electronic and ionic charges in doped PEDOT:PSS, thereby de-doping the channel and gate (we note that other cations in solution such as Na^+ or K^+ may compensate PSS^- instead of or in addition to H^+). **b**, This reaction at the gate electrode (1) changes its potential, resulting in effective gating of the PEDOT:PSS postsynaptic channel, and results in a transfer of an electron and a proton to the postsynaptic channel (2) to maintain to a potential drop of V_{post}. **c**, To test this hypothesis, a device structure as shown in **b**, is fabricated and the conductance of both the postsynaptic electrode and postsynaptic channel are measured before and after oxidation driven at the postsynaptic electrode. The conductance of both the postsynaptic channel and electrode decrease, confirming the transfer of protons (or cations) and electrons to both PEDOT:PSS electrodes.

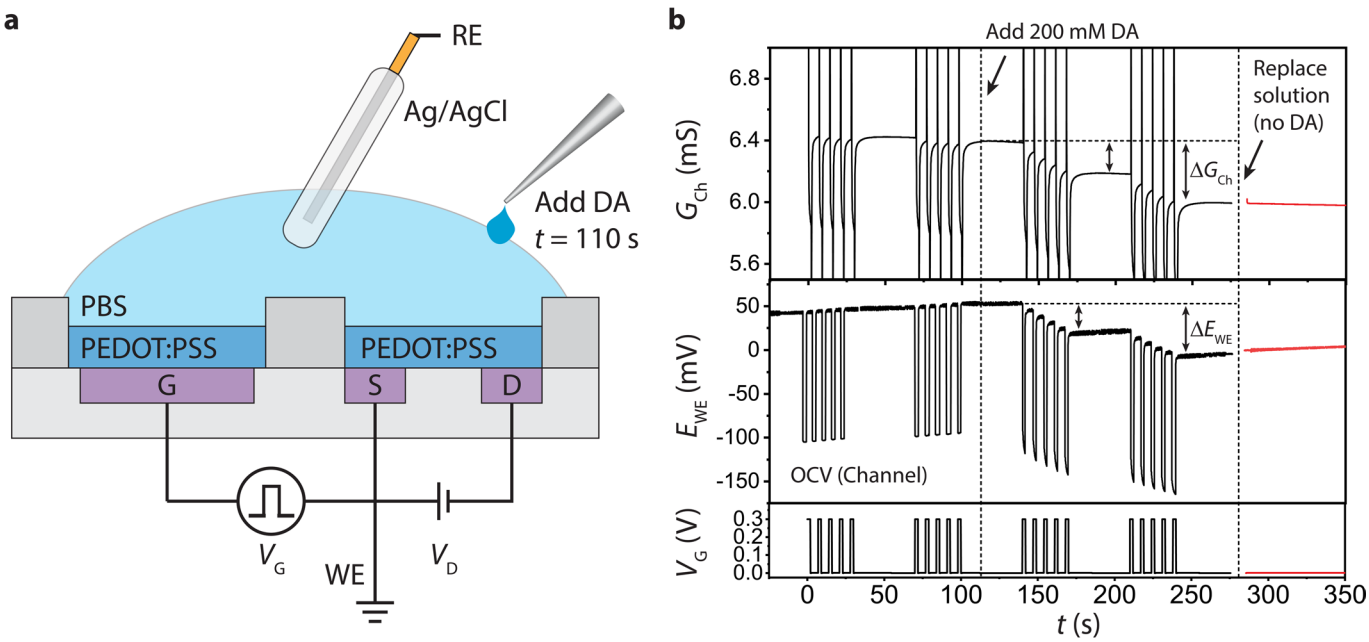

Extended Data Fig. 4 | Potential change of PEDOT:PSS channel following dopamine oxidation. a, Schematic of the experimental setup for monitoring the potential of the PEDOT:PSS channel during device operation using a potentiostat operated in open circuit voltage mode. The channel is connected to a grounded working electrode (WE) and the potential is monitored in reference to a saturated silver/silver chloride (Ag/AgCl) reference electrode (RE) immersed in the electrolyte. **b**, The channel conductance (G_{Ch}), potential (E_{WE}) and gate voltage pulses (V_G) over time showing no change in G_{Ch} or E_{WE} in the absence of dopamine (DA) in response to V_G pulses. After DA is added to solution, G_{Ch} and E_{WE} both decrease in response to V_G pulses, showing the change in G_{Ch} (ΔG_{Ch}) is due to the potential change in the channel following oxidation (ΔE_{WE}). At t = 275 s, we exchange the solution with fresh PBS containing no DA to show that both ΔE_{WE} and ΔG_{Ch} are properties of the channel, not the solution.

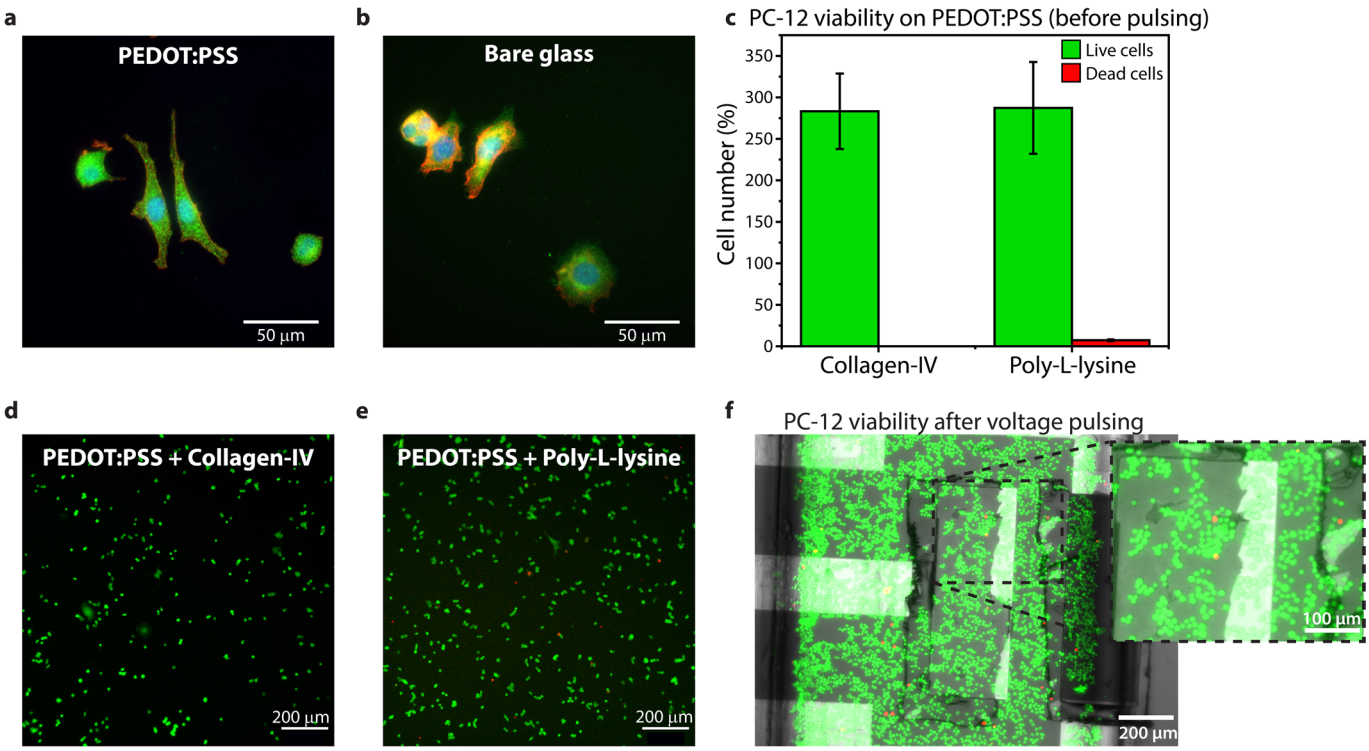

Extended Data Fig. 5 | Dopamine immunohistochemistry and biocompatibility for PC-12 cells on PEDOT:PSS. The figure reports a comparison between PC-12 cells seeded on PEDOT:PSS film **a**, and bare glass **b**. In both cases the green fluorescence confirmed the presence of dopamine released locally at the cell membrane (in red), showing that dopamine is produced in vesicles in the PC-12 cells and then released. **c**, The viability of PC-12 cells was tested by staining live cells with calcein-AM (green) and dead cells with propidium iodide (red) for PEDOT:PSS electrodes coated with **d**, collagen IV and **e**, poly-L-lysine films. Both substrates exhibited good cell viability, with the collagen-IV coated film showing higher biocompatibility. For this reason, the collagen-IV coating was employed in all of the following experiments. **f**, Live/dead staining performed on PC-12 cells inside the microfluidic channel after performing repeated pulsed electrical measurements, showing no difference between cells cultured on PEDOT:PSS **e**, prior to and **f**, following electrical measurements, indicating no alteration of cell viability from the electrical measurements.

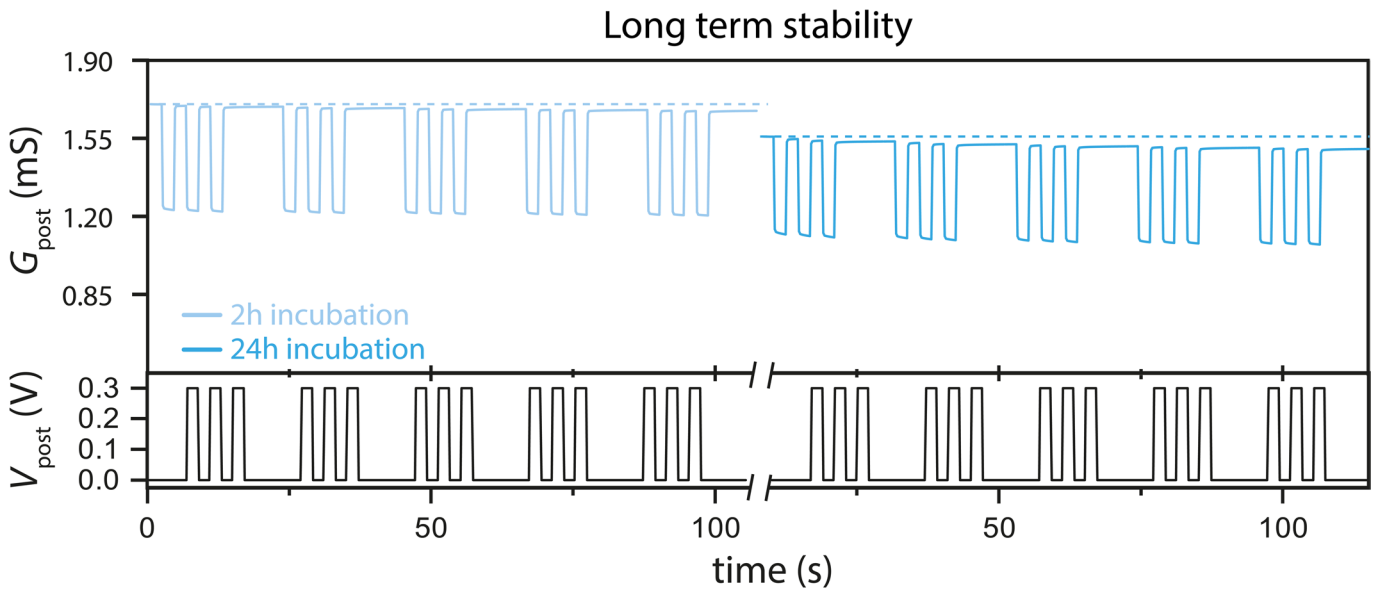

Extended Data Fig. 6 | Long-term device stability. Comparison of pulsed measurements performed on the biohybrid synapse after 2 hours (light blue line) and after 24 hours (blue line) following cell plating. The efficiency of the device remains unaltered since synaptic plasticity behavior from dopamine oxidation is retained following extended exposure to the cell culture media.

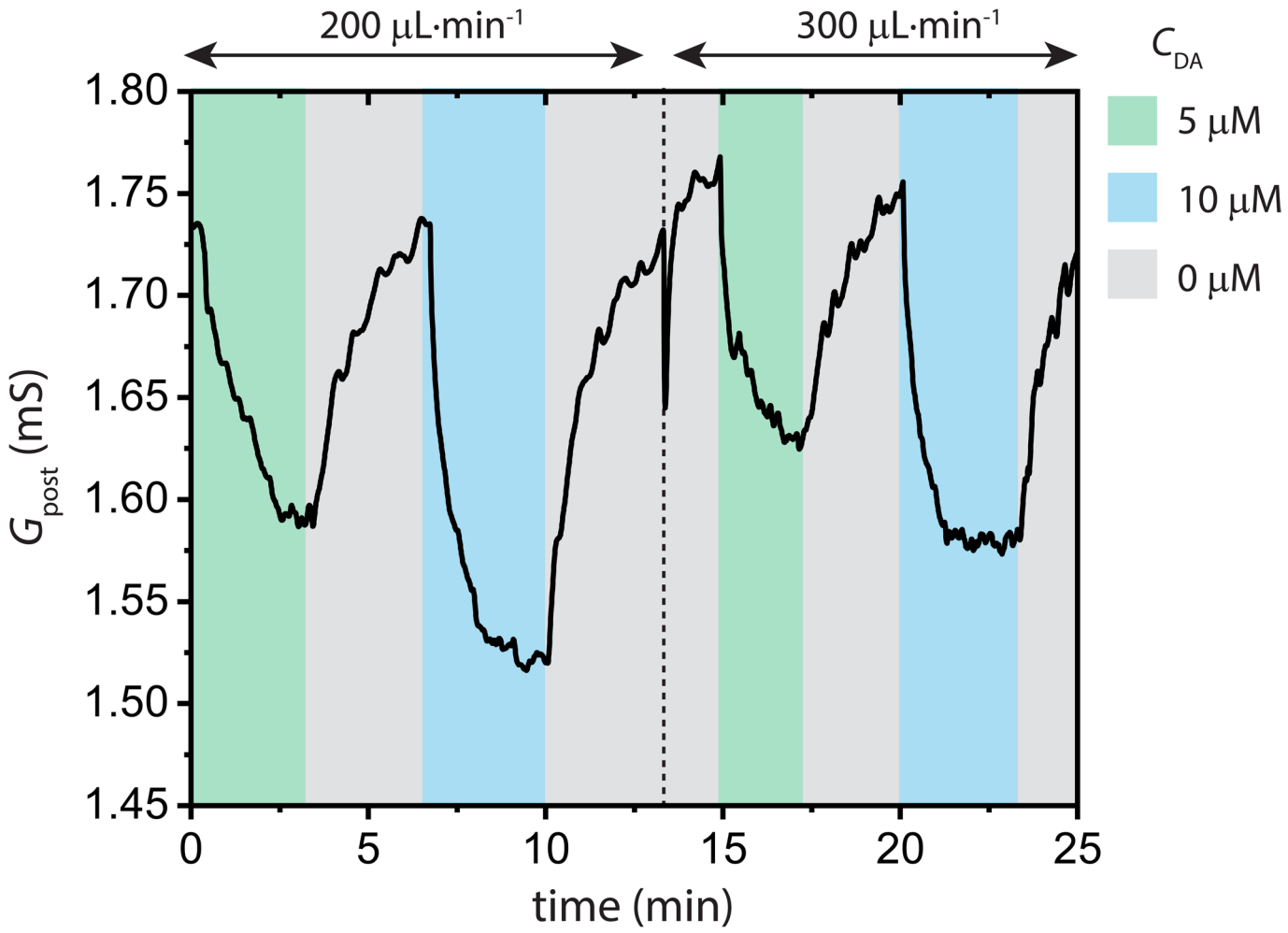

Extended Data Fig. 7 | Steady state dopamine detection with variable flow rate. Steady-state measurements of the postsynaptic channel conductance (V_{post} = +0.3 V, V_{ch} = -0.2 V) under varied flow rates and dopamine concentrations. When the flow rate is increased from 200 μL min^{-1} to 300 μL min^{-1}, the equilibrium G_{post} is larger for the same dopamine concentration. Additionally, the recovery time for the higher flow rate is shorter due to the fact that the fresh solution carries oxygen which can oxidize the PEDOT:PSS postsynaptic channel at faster rates when the solution flow rate is increased.

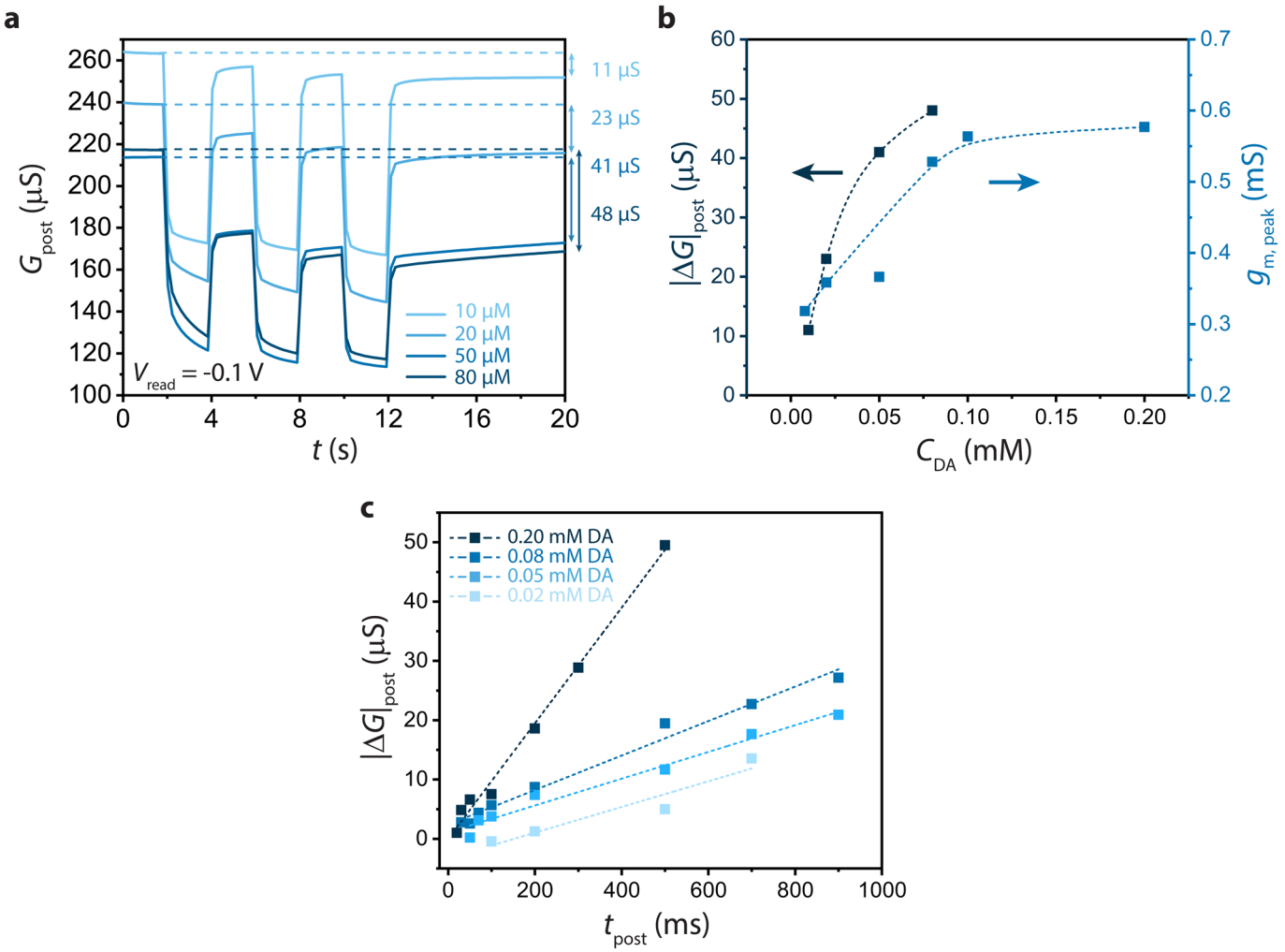

Extended Data Fig. 8 | Calibration of the organic neuromorphic device with increasing dopamine concentration. a, Pulsed measurements of the *ex vivo* neuromorphic device under microfluidic flow of DMEM solution at varied dopamine concentrations showing the postsynaptic conductance change following voltage pulses with increasing dopamine concentration. **b**, Calibration curve showing the conductance change during pulsing (left, dark blue) and peak transconductance during transfer measurements (right, light blue) as a function of increasing dopamine concentration. **c**, Postsynaptic channel conductance update as a function of gate voltage pulse width for the *ex vivo* neuromorphic device with varied dopamine concentrations showing a nearly linear time dependence for all concentrations. The minimum pulse width resulting in a change in postsynaptic current (LTP) also depends on the dopamine concentration; at 0.02 mM the pulse width must be >100 ms to elicit a response, whereas at 0.2 mM a pulse width of 10 ms is sufficient to cause LTP.

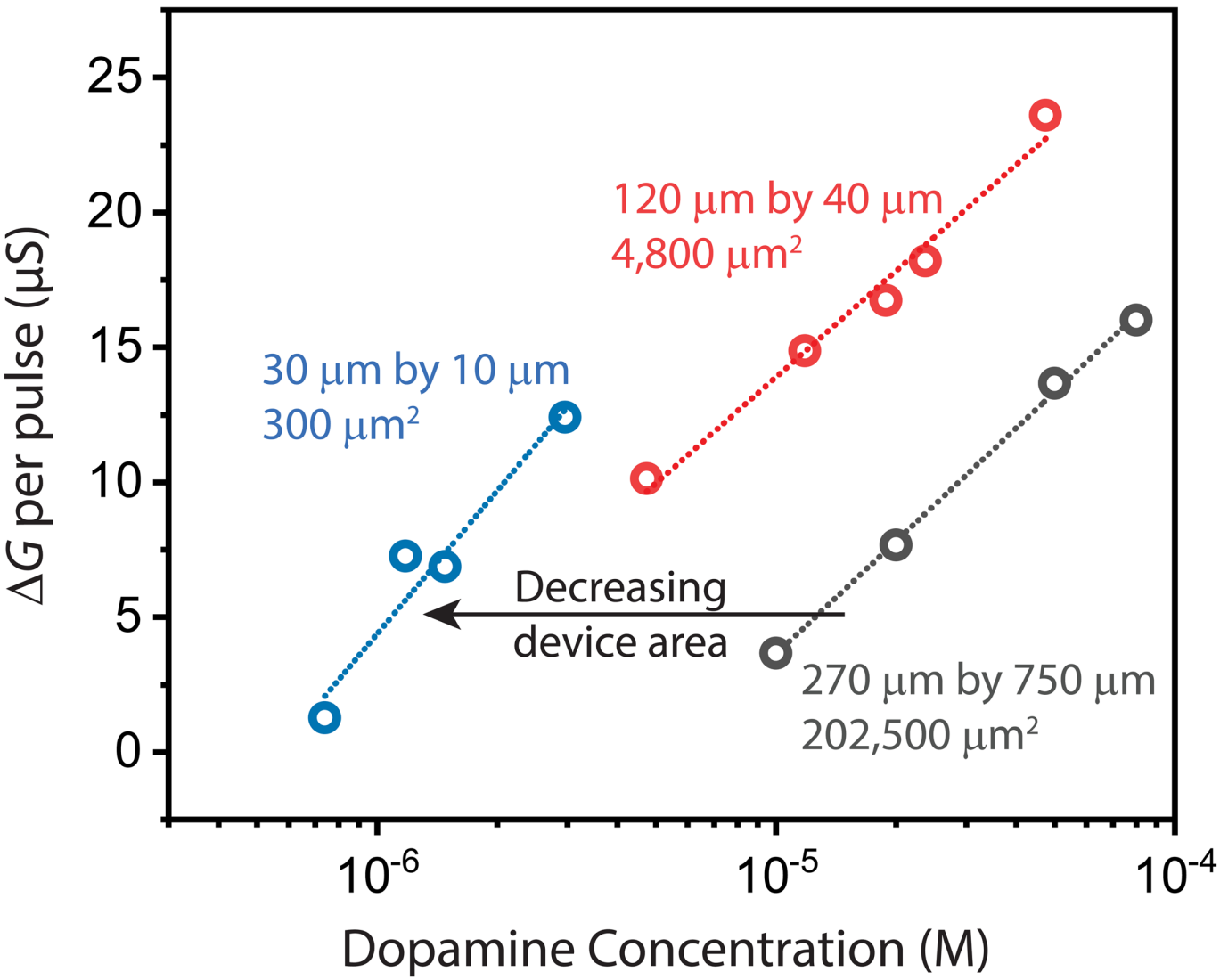

Extended Data Fig. 9 | Dopamine response of scaled neuromorphic devices. As the neuromorphic device electrode area is decreased, the conductance change per pulse (V_{pulse} = 0.3 V, t_{pulse} = 2 s) increases proportionally. Measurements are performed in the absence of microfluidic flow.